[Research Paper] 대한금속 · 재료학회지 (*Korean J. Met. Mater.*), Vol. 57, No. 11 (2019) pp.732-740
DOI: 10.3365/KJMM.2019.57.11.732

Low-Temperature H_2S Sensors Based on Si-Coated SnO_2 Nanowires

Myung Sik Choi[1], Ali Mirzaei[2,3], Jae Hoon Bang[1], Han Gil Na[1], Changhyun Jin[1,2], Wansik Oum[1], Seungmin Han[1], Sang Sub Kim[4,*], and Hyoun Woo Kim[1,2,*]

[1]*Division of Materials Science and Engineering, Hanyang University, Seoul 04763, Republic of Korea*
[2]*The Research Institute of Industrial Science, Hanyang University, Seoul 04763, Republic of Korea*
[3]*Department of Materials Science and Engineering, Shiraz University of Technology, Shiraz, Iran*
[4]*Department of Materials Science and Engineering, Inha University, Incheon 22212, Republic of Korea*

Abstract: To attain high life standards, it is important to develop high-performance non-toxic gas sensors for public safety, environmental pollutant control, industrial processes, etc. Because reports on single element semiconductor-coated semiconducting metal oxides for sensing applications are rare, we synthesized SnO_2 nanowires and coated them with a 5 nm-thick or 10 nm-thick Si layer for H_2S gas sensing studies. SnO_2 nanowires were successfully synthesized using a highly pure metallic Sn powder at high temperature in a tube furnace by the vapor-liquid-solid method and Si was deposited on the nanowires by the sputtering technique. The desired morphology and composition of the synthesized nanowires were confirmed by scanning electron microscopy, transmission electron microscopy, X-ray diffraction, and energy-dispersive X-ray spectroscopy. Moreover, the gas sensing characteristics of pristine and Si-coated SnO_2 nanowires toward H_2S, CO, H_2, C_6H_6, C_2H_5OH and C_6H_7 gases were investigated. The sensing results revealed a good response to H_2S at the optimum operational temperature of 100 °C. Notably, Si-coated SnO_2 nanowire sensors showed a better response to H_2S than pristine SnO_2 nanowires. The mechanism of H_2S sensing is discussed in detail here. This study shows that the Si coating on the SnO_2 nanowire enhances its sensing performance and decreases the sensing temperature required for H_2S gas detection.

(Received May 3, 2019; Accepted September 7, 2019)

Keywords: SnO_2, nanowires, Si, coating, H_2S, gas sensor, semiconductor

1. INTRODUCTION

The considerable demand for materials with enhanced properties that can satisfy the requirements of modern technology in the 21st century has resulted in the development of one-dimensional nanomaterials such as nanowires [1], nanorods [2], and nanofibers [3]. Their high aspect ratios as well as good electrical, mechanical, chemical, and thermal properties [4] have led to their application in batteries [5], photocatalysts [6], fuel cells [7], gas sensors [8], etc. Gas adsorption strongly depends on the number of available adsorption sites; because nanowires provide very high surface areas for gas adsorption, they have found particular attention in the field of gas sensors. Notably, nanowire-based gas sensors exhibit high sensitivity, short response times, and high stability; in addition, they are lightweight and can operate at lower temperatures than sensors fabricated from their bulk counterparts [9]. Therefore, several nanowire-based gas sensors have been developed [10-13]. Stannic oxide (SnO_2) is one of the most important n-type semiconducting (E_g ~ 3.6 eV) metal oxides [14] and has been used in gas sensors [15-17]. However, its working temperature is often high and it generally shows poor selectivity [18,19]. To address these issues, the morphology of SnO_2 nanowires has been altered [20] and n-p junctions based on composites of SnO_2 and other p-type metal oxides [21] have been fabricated. SnO_2-Si heterojunction nanowires are promising materials for gas sensing applications. Si-based gas sensors [11] have currently received significant interest for gas sensing because of their

- Myung Sik Choi: 박사과정, Ali Mirzaei·Changhyun Jin·Sang Sub Kim·Hyoun Woo Kim: 교수, Jae Hoon Bang: 석박사통합과정, Wansik Oum·Seungmin Han:석사과정
**Corresponding Author:* Sang Sub Kim
[Tel: +82-82-32-960-7546, E-mail: sangsub@inha.ac.kr]
**Corresponding Author:* Hyoun Woo Kim
[Tel: +82-2-2220-0382, E-mail: hyounwoo@hanyang.ac.kr]

low working temperatures [10] and compatibility with silicon technology [22]; however, their response is low [23] and their performance needs to be improved. In the case of a SnO_2-Si sensor, SnO_2 provides enhanced sensing characteristics while Si decreases the working temperature, making the sensor highly compatible with silicon technology. Some researchers have investigated composites of Si with other metal oxides for sensing applications. For example, Zhang et al. [24] fabricated an NO_2 gas sensor based on Si/WO_3 nanowires that functioned at room temperature. Liu et al. [25] reported NO_2 gas sensing with CuO/p-porous silicon heterojunctions at room temperature. However, to the best of our knowledge, H_2S sensing properties of Si-coated SnO_2 nanowires have not been investigated. In this work, Si-coated SnO_2 nanowires were synthesized by thermal evaporation, and then, Si was sputtered on the nanowires. The fabricated Si-coated SnO_2 nanowires demonstrated an enhanced response to H_2S compared to pristine SnO_2 nanowires. The sensing mechanisms are explained in detail in this report.

2. EXPERIMENTAL PROCEDURE

2.1 Synthesis

SnO_2 nanowires were produced in a tube furnace. For the synthesis, metallic Sn nanopowder with a purity of 99.9% was used as the raw material. Typically, a 3 nm-thick Au layer was coated on a Si substrate as catalyst; the Au-coated substrate was heated at 900 °C for 1 h, and then, exposed to a mixture of Ar (97%) and O_2 (3%) gases at a constant flow rate and total pressure of 2 Torr. The details of the SnO_2 nanowire synthesis have been reported in our previous publications [26,27].

Si was coated on the as-grown SnO_2 nanowires by radio frequency (RF) sputtering with a Si target at room temperature. The optimal pressure for the Si shell layer deposition was 10 mTorr in Ar ambient and the RF power during the deposition was set to 50 W. The sputtering time was varied from 2 min to 4 min to obtain Si shells with thicknesses of 5 nm and 10 nm, respectively.

2.2 Material Characterization

The crystallinity and phase purity of the prepared samples were investigated by X-ray diffraction (XRD) using a Philips X'Pert diffractometer with the Cu $K_{\alpha 1}$ radiation (λ = 1.5404 Å). The morphology was investigated by scanning electron microscopy (SEM, Hitachi S-4200) and transmission electron microscopy (TEM, Philips CM 200). Energy-dispersive X-ray spectroscopy (EDS) was performed to study the chemical composition of the synthesized products. The work function of SnO_2 nanowires was determined from the ultraviolet photoelectron spectroscopy (UPS) profiles recorded using an HeI (21.2 eV) ultraviolet source.

2.3 Sensor Fabrication and Gas Sensing Tests

Details of the gas sensing tests can be found elsewhere [28-30]. A bi-layered electrode comprising a Au layer (300 nm-thick) and a Ti layer (50 nm-thick) was sputter-deposited on each sample. The gas flow was controlled by changing the mixing ratio of dry air to the target gas using mass flow controllers under a total stream of 500 sccm. All measurements were carried out in a special gas chamber and the sensor resistance data were obtained using a source meter. The sensor response (R) is defined as $R = R_a/R_g$, where R_a and R_g are the resistances of the sensor in air and in the presence of the target gas, respectively. The response and recovery times were calculated as the time to reach 90% of the final signal after exposure and stoppage of the target gas, respectively.

3. RESULTS AND DISCUSSION

3.1 Morphological and Structural Studies

The morphology of the synthesized nanowires was studied by SEM and the micrographs are presented in Fig. 1 (a)-(f). Fig. 1(a) reveals bare, curvy, and continuous SnO_2 nanowires with lengths in the order of several micrometers and diameters of ~100 nm. Figure 1(b) is a high-magnification SEM image showing the smooth morphology of the synthesized bare SnO_2 nanowires. Figure 1(c) shows Si-coated SnO_2 nanowires with a shell thickness of 5 nm and the high-magnification SEM image in Fig. 1(d) shows the relatively smooth morphology of the coated nanowires. Figure 1(e) and (f) show the SEM images of Si-coated (10 nm) SnO_2 nanowires. Coating with a 10 nm Si shell resulted in a relatively rough morphology.

To determine the crystal structure of the synthesized

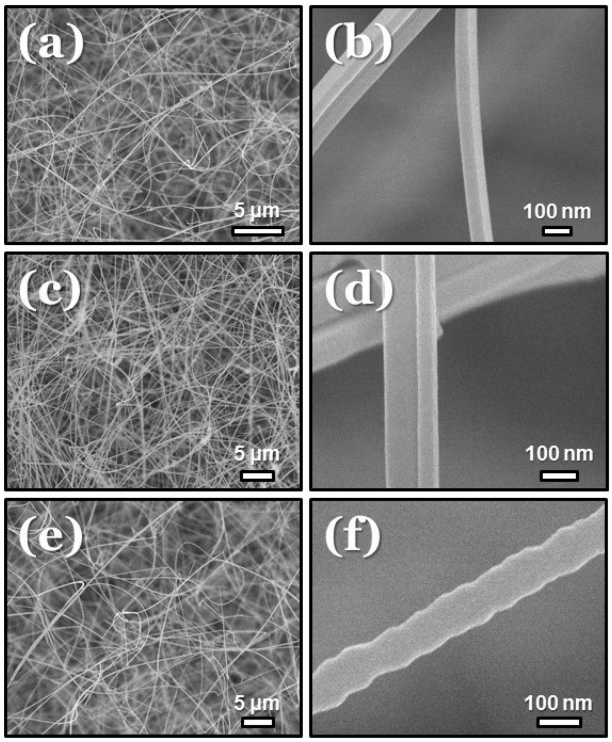

Fig. 1. SEM images of (a) and (b) bare SnO_2 nanowires, (c) and (d) SnO_2 nanowires with 5 nm-thick Si shells, and (e) and (f) SnO_2 nanowires with 10 nm-thick Si shells.

nanowires, XRD patterns of bare and Si-coated SnO_2 nanowires were recorded and are shown in Fig. 2(a)-(c).

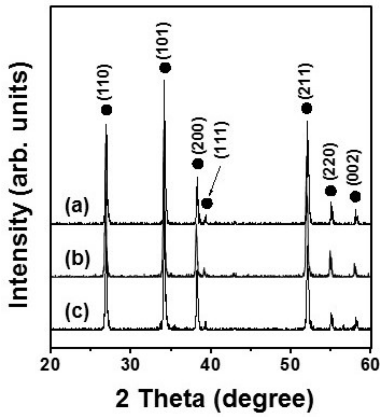

Fig. 2. XRD patterns of (a) bare SnO_2 nanowires and SnO_2 nanowires with Si shell thicknesses of (b) 5 nm and (c) 10 nm.

Common peaks for all materials were observed at 2θ = 26.61, 33.92, 37.99, 39.02, 51.83, 54.81, and 57.91°, corresponding to the (110), (101), (200), (111), (211), (220), and (002) planes of SnO_2, respectively. Si peaks at 2θ = 26.87 (200), 33.07 (211), 38.37 (220), 51.53 (321), 55.38 (400), and 59.06° (411), originating from the Si shell, overlapped with the SnO_2 peaks. In addition, the microstructures of bare and Si-coated SnO_2 nanowires were studied by TEM and the micrographs are presented in Fig. 3. TEM images of SnO_2 nanowires with shell thicknesses of 5 nm and 10 nm are shown in Fig. 3(a) and 3(d), respectively. As observed, the

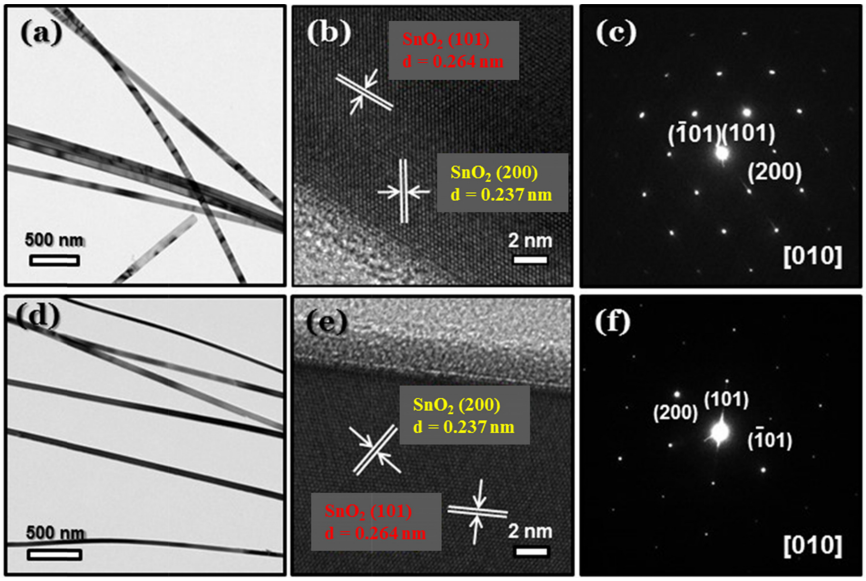

Fig. 3. (a) TEM and (b) HRTEM images and (c) SAED pattern of SnO_2 nanowires with a shell thickness of 5 nm. (d) TEM and (e) HRTEM images and (f) SAED pattern of SnO_2 nanowires with a shell thickness of 10 nm.

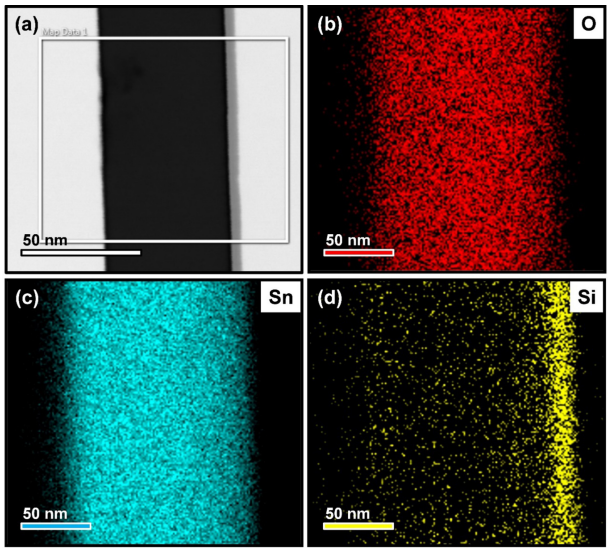

Fig. 4. EDS elemental mapping images showing the presence of Si, Sn, and O.

nanowires were long and separate from one other, suggesting that they can provide high surface areas for gas adsorption. The diameters of the nanowires were about 100 nm, in accordance with the SEM results. The high-resolution TEM (HRTEM) images of SnO_2 nanowires with shell thicknesses of 5 nm and 10 nm are shown in Fig. 3(b) and 3(e), respectively. In both cases, lattice fringes with spacings of 0.264 nm and 0.237 nm, corresponding to the (101) and (200) planes of SnO_2, respectively, were observed. This result further confirmed the crystalline nature of the SnO_2 nanowires. The corresponding selected area diffraction (SAED) patterns showing distinct diffraction spots are presented in Fig. 3(c) and 3(f) which confirms the single crystalline nature of the synthesized SnO_2 nanowires. The EDS elemental mapping images revealing the presence Si, Sn, and O in the synthesized nanowires are shown in Fig. 4. It is noteworthy that a thin Si layer covered the SnO_2 nanowires.

3.2 Gas Sensing Studies

From a series of preliminary tests, we determined that the optimal working temperature of the sensors was 100 °C; therefore, all gas sensing measurements were performed at 100 °C. Fig. 5 shows the H_2S sensing properties of bare and Si-coated SnO_2 nanowires. The dynamic response plots of bare SnO_2 nanowires for 10, 20, and 50 ppm of H_2S gas are shown in Fig. 5(a). Upon exposure to H_2S gas, the resistance

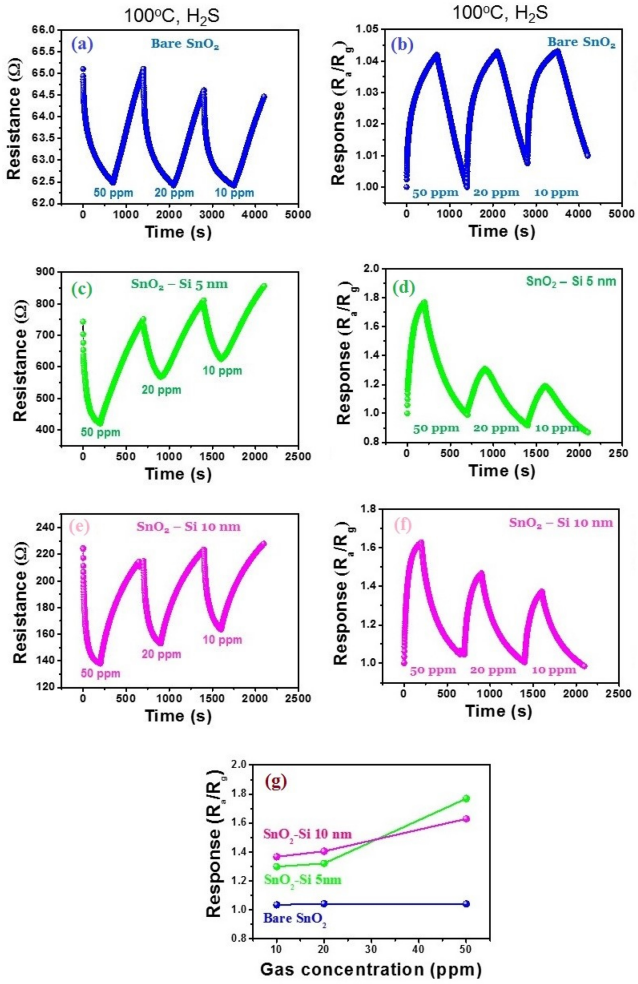

Fig. 5. Dynamic responses of (a) bare SnO_2 nanowires and SnO_2 nanowires with Si shell thicknesses of (c) 5 nm and (e) 10 nm toward 10, 20, and 50 ppm of H_2S gas at 100 °C. Response of (b) bare SnO_2 nanowires and SnO_2 nanowires with shell thicknesses of (d) 5 nm and (f) SnO_2 10 nm toward 10, 20, and 50 ppm of H_2S gas at 100 °C. (g) Corresponding calibration curves.

of the sensor decreased, reflecting its n-type behavior. Furthermore, the response was reversible, because after stopping the injection of H_2S and air, the resistance returned to its initial value. The response (R_a/R_g) versus time plots are presented in Fig. 5(b). The responses of the bare SnO_2 nanowire sensor to 10, 20, and 50 ppm H_2S gas were 1.035, 1.043, and 1.043, respectively, indicating that the response was almost identical for different concentrations of H_2S gas. This was likely due to the limited surface area of the bare SnO_2 nanowire. The dynamic response plots of 5 nm-thick and 10 nm-thick Si shell-coated SnO_2 nanowires for different concentrations of H_2S are shown in Fig. 5(c) and 5(e),

respectively. Both sensors showed n-type behaviors and reversible responses. Fig. 5(d) and 5(f) show plots of response as a function of time for SnO_2 nanowires coated with 5 nm- or 10 nm-thick Si shells. The responses of SnO_2 nanowires with 5 nm Si shells to 10, 20, and 50 ppm of H_2S gas were 1.299, 1.321, and 1.769, respectively, while those of SnO_2 nanowires with 10 nm-thick Si shells were 1.367, 1.405, and 1.629, respectively. The calibration curves of all sensors are shown in Fig. 5(g). Clearly, the response of bare SnO_2 nanowires was far lower than that of Si-coated SnO_2 nanowires. This demonstrated that Si enhanced the sensing performance of the SnO_2 nanowire. Furthermore, the nanowires with 5 nm-thick Si shells showed a higher response to 50 ppm of H_2S than those with 10 nm-thick shells; on the other hand, to 10 ppm and 20 ppm of H_2S, the response of nanowires with 5 nm-thick Si shells was higher.

Selectivity for a target gas is highly important for real applications because a lack of selectivity can lead to false alarms, limiting the practical application of a sensor. To study the selectivity of 5 nm-thick Si shell-coated SnO_2 nanowires, they were exposed to 50 ppm of benzene, ethanol, CO, H_2, and toluene gases at 100 °C. Fig. 6(a) shows the variations in responses to these gases with time; the corresponding selectivity histogram of the sensor is presented in Fig. 6(b). The sensor responses to the gases were 1.051, 1.028, 1.052, 1.047, and 1.016, respectively, indicating that these sensors were largely insensitive to interfering gases.

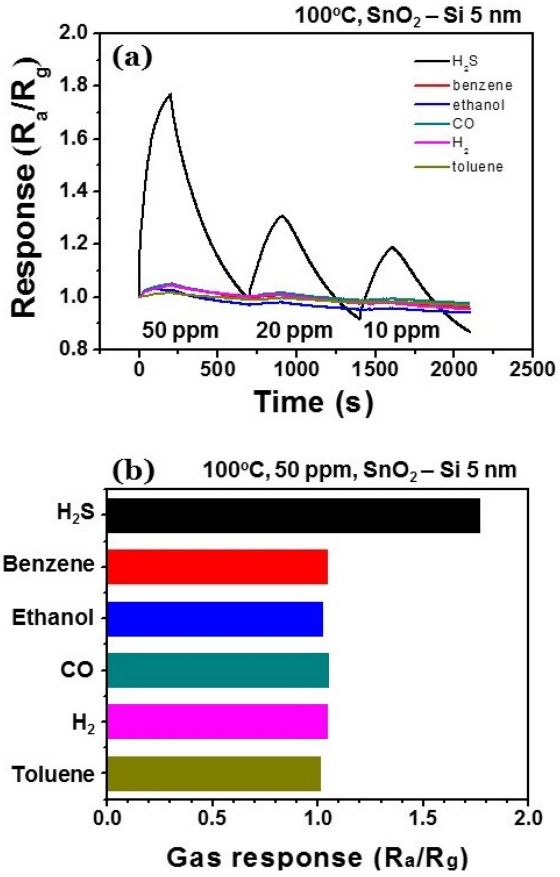

Fig. 6. (a) Transient response of SnO_2-Si (10 nm) sensor toward different gases at 100 °C. (b) Selectivity histogram of SnO_2-Si (5 nm) sensor to 50 ppm of gases tested at 100 °C.

3.3 Gas Sensing Mechanism

Several factors can influence the sensing behavior of Si-shelled SnO_2 nanowires. When considering the changes in the resistance of a SnO_2-Si core-shell nanowire upon exposure to H_2S gas, the change in the resistance of the SnO_2 nanowire core (R_1) and the change in the resistance of the Si shell (R_2) should be taken into account [28]. Almost every gas adsorbs onto the surface of a metal oxide [31]. The most prominent reactive gas in normal ambient air is molecular oxygen. Depending on the sensor operation temperature, oxygen adsorbs in various forms onto the metal oxide surface. Exposure of a pristine SnO_2 nanowire sensor to air results in the adsorption of oxygen molecules onto the surface of the nanowire. Because of the high electron affinity of oxygen, the adsorbed oxygen molecules trap electrons from the conduction band of SnO_2, forming ionized oxygen species such as O_2^-, O^-, and O^{2-} [2]:

$$O_{2(gas)} \rightarrow O_{2(ads)} \quad (3)$$

$$O_{2(ads)} + \bar{e} = O^-_{2(ads)} \quad (4)$$

$$O^-_{2(ads)} + \bar{e} = 2O^-_{(ads)} \quad (5)$$

$$O^-_{(ads)} + \bar{e} = O^{2-}_{(ads)} \quad (6)$$

Consequently, the concentration of electrons on the surface decreases, and accordingly, the resistance of the SnO_2 nanowires increases. When a pristine SnO_2 nanowire gas sensor is exposed to H_2S, H_2S molecules chemisorb on the surface of the SnO_2 nanowire, and electrons are released by a subsequent reaction with oxygen ions, resulting in H_2O and SO_2 gases [32]:

$$H_2S_{(ads)} + 3O^-_{(ads)} = SO_{2(g)} + H_2O + 3\bar{e} \quad (7)$$

The released electrons decrease the resistance of the gas sensor, resulting in a response. Because the core SnO_2 nanowires were single crystalline, the effects of grain boundaries were excluded. After Si was coated on the SnO_2 nanowires, an increase in response was observed. As observed in Fig. 5(g), the response of the Si-shelled nanowires was superior to that of bare nanowires, regardless of the gas concentration or shell thickness. The H_2S gas sensing mechanism for the Si-coated SnO_2 nanowire sensor can be explained on the basis of several factors. The TEM results revealed that the Si shell layer did not completely cover the core nanowire, wherein a part of the core was exposed along the entire length of the nanowire. More importantly, the sensor exhibited an n-type behavior, illustrating the dominant role of the SnO_2 nanowire core in sensing.

Similar to that for the SnO_2 nanowires, adsorption of H_2S gas likely changed the resistance of the Si shell layer. When SnO_2 nanowires with Si shell layers were exposed to H_2S, electrons were released, as shown in Eq. (7). Because the Si shell layer had a p-type semiconducting property, the adsorption of H_2S gas resulted in the donation of electrons or extraction of holes, generating a hole depletion region. Thus, when H_2S gas was introduced, the resistance of the Si shell layer increased. Furthermore, because the Si shell layer was polycrystalline, modulation of resistance might occur along grain boundaries.

An important difference between the pristine and Si-coated SnO_2 nanowire sensors is the existence of Si-SnO_2 p-n junctions. Notably, SnO_2/Si heterointerfaces affect the sensing behavior. In particular, the conductivity, accumulation of electrons, and size of the electron depletion region prior to H_2S introduction will determine the sensor response. The work function of SnO_2 is reported to be in the range of 4.0-5.7 eV [33-47]. In this study, the work function of SnO_2 nanowires was measured to be 4.8 eV. From the UPS profile of SnO_2, the cut-off value was determined to be 16.5 eV (Fig. 7). The work function was calculated by subtracting the cut-off value from the reference value of 21.1 eV. To correct the broadening due to the analyzer, 0.1 eV was added to each work function value. Accordingly, the work function of the SnO_2 nanowire was calculated to be 4.8 eV (= 21.2 eV – 16.5 eV + 0.1 eV). Previous studies have reported that the work function of Si falls within the range of 4.1-5.0 eV [48-60]. In particular, the

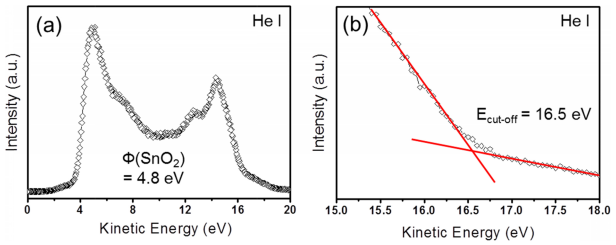

Fig. 7. (a) UPS profile of SnO_2 nanowires. (b) Calculation of cut-off value.

work function of p-type Si is 4.7-5.0 eV [59]. There are two possible explanations for the enhanced response observed in the presence of the Si shell, both of which depend on the relative magnitudes of the work functions.

One possibility is that the Fermi level (E_F) of p-Si is higher than that of SnO_2. In this case, the work function of SnO_2 will be larger than that of p-Si. Therefore, electrons from p-Si will flow to SnO_2 to balance the Fermi levels. At the same time, holes from SnO_2 will flow to p-Si. Consequently, electron and hole accumulation layers will be generated on the SnO_2 and p-Si sides of the heterojunction, respectively. Subsequently, the conduction volume of the SnO_2 core will increase and a corresponding change in the conduction volume due to the introduction/removal of H_2S gas will generate a lower sensor response. The other possibility is that the Fermi level (E_F) of p-Si is lower than that of SnO_2 (Fig. 8(a)). In this case, the work function of SnO_2 will be smaller than that of p-Si. Thus, electrons from SnO_2 will flow to p-Si (Fig. 8(b)). Consequently, electron and hole depletion layers will be generated on the SnO_2 and p-Si sides of the heterojunction, respectively. Subsequently, the initial conduction volume in the SnO_2 core will decrease and a corresponding change in the conduction volume due to the introduction/removal of H_2S gas will generate a higher sensor response. As observed in Fig. 5(g), the addition of the Si shell layer enhanced the response of the bare nanowire sensor, indicating that the work function of SnO_2 was smaller than that of p-Si in this work. Moreover, the deposition of Si onto the SnO_2 nanowires might introduce structural defects, favoring the adsorption of the target gas as well as oxygen molecules, and thereby, leading to an increase in the sensor signal [29].

A schematic diagram of the sensing mechanism for the fabricated sensors is given in Fig. 9. Notably, the TEM results showed that the shell layer was partially open, in other

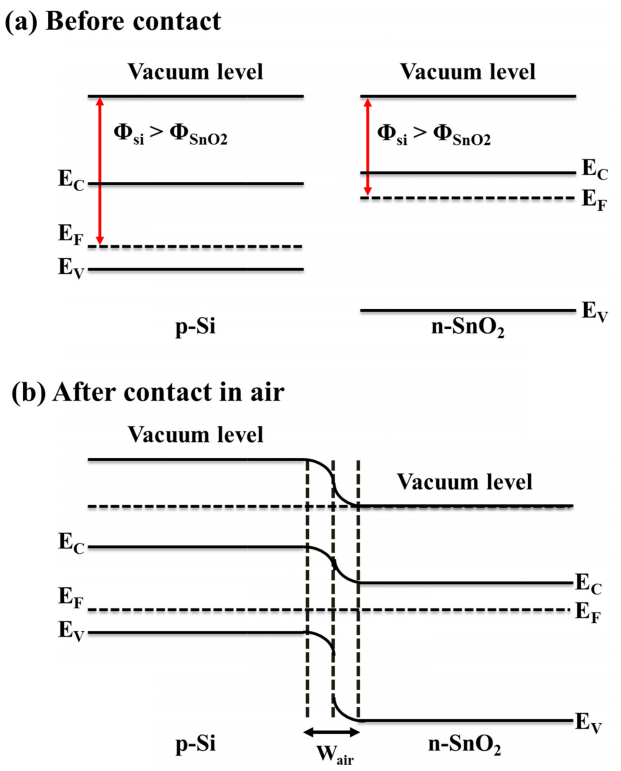

Fig. 8. (a) Band structure of n-SnO_2 and p-Si before contact and (b) after contact in air.

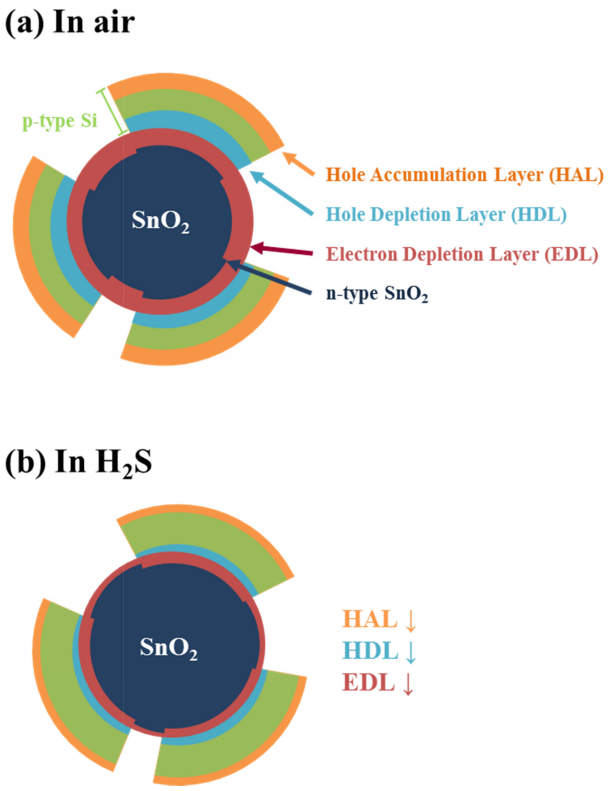

Fig. 9. Schematic illustration of variation in the conduction channel of SnO_2 nanowire coated with Si in (a) air and (b) H_2S atmospheres. (HAL: hole accumulation layer, HDL: hole depletion layer, EDL: electron depletion layer)

words, the shell layer partially covered the core SnO_2 nanowire. Because the shell was preferentially deposited on one side of the core nanowire, the shell was partially open and a considerable part of the SnO_2 core was exposed to air ambient. Accordingly, electron currents in the n-SnO_2 core and hole currents in p-Si contributed to the sensing behavior. Because of the work function difference between Si and SnO_2 in air and exposure of the bare surfaces to air, a hole accumulation layer, a hole depletion layer, and an electron depletion layer were formed (see Fig. 9(a)). As shown in Fig. 9(a), the hole and electron depletion layers were formed on the p-Si and n-SnO_2 sides, respectively, at the interface between p-Si and n-SnO_2. Upon exposure to H_2S, electrons returned to the surface of the sensing layer, decreasing the width of the electron and hole depletion layers and the hole accumulation layer, as shown in Fig. 9(b).

The introduction of H_2S gas resulted in a decrease in the resistance of both bare and Si-coated SnO_2 nanowire sensors. Thus, the sensors exhibited n-type behaviors. Accordingly, we surmised that the main sensing current was the electron current flowing through the n-type SnO_2 nanowire core, although both electron and hole currents flowed; notably, a change in the transport mode enhanced the sensing behavior.

To the total resistance induced by introduction of H_2S, the contribution by the SnO_2 core was higher than that by the Si shell. Because sensor total current comprises an SnO_2 core and a Si-shell in parallel, the equivalent resistance R_{eq} could be defined by the following equation: $1/R_{eq} = 1/R_n + 1/R_p$, where R_n and R_p are the resistances of the n-type core and p-type shell, respectively. Because the total resistance (equivalent resistance) was smaller than R_n and R_p, the simultaneous presence of the SnO_2 core and Si-shell generated a higher sensor response.

As shown in Fig. 6, the fabricated sensor exhibited selectivity toward H_2S gas. The Si shell layer contributed to enhancement of the sensing activity of the sensor. The Si shell was covered with a thin native oxide (SiO_x) layer due to the exposure of the Si shell to air. This resulted in a

significant decrease in the sensing activity, because of insulating characteristics of silicon oxide. Thus, possibly H_2S gas molecules attacked and partially removed the SiO_x layer. Another possibility is that H_2S decomposed, generating H_2 gas species by the following reaction: $2H_2S \rightarrow 2H_2 + S_2$. This reaction has been reported to easily occur at high temperatures in the presence of metal catalysts, sulfide catalysts, and sulfur bacteria [30]. Although the sensing temperature in the present work was not high, possibly SnO_2 or interstitial Sn played a catalytic role in the decomposition of H_2S. The generated H_2 might have reacted with SiO_x, leading to the removal of the silicon oxide layer. The other possibility is that H_2S gas molecules directly reacted with the silicon oxide layer according to the following reaction: $SiO_2 + 2H_2S \rightarrow SiS_2 + 2H_2O$. However, the Gibbs free energy for the above reaction is positive at the sensing temperature of 100 °C; therefore, the direct reaction of H_2S with the native oxide would not have contributed to the removal of the oxide layer [61,62].

4. CONCLUSIONS

In conclusion, uncoated and Si-coated (5 nm and 10 nm) SnO_2 nanowires were synthesized and their gas sensing performances were investigated. At the optimal operation temperature (100 °C), the response of Si-coated SnO_2 nanowires to H_2S was higher than that of bare SnO_2 nanowires. The responses of SnO_2 nanowires with 5 nm-thick Si shells and 10 nm-thick Si shells were highly similar. However, at a high H_2S concentration (50 ppm), the response of SnO_2 nanowires with 5 nm-thick Si shells was higher than that of SnO_2 nanowires with 10 nm-thick Si shells (1.769 versus 1.629). The removal of the native SiO_x layer by H_2S gas, creation of p-n heterojunctions, modulation of the conduction channels of both SnO_2 and Si, and creation of imperfections in Si-coated SnO_2 nanowires were the main reasons for the improved response to H_2S gas. Si-coated SnO_2 nanowire sensors were tested in other gas atmospheres, and the sensors revealed good selectivity to H_2S gas compared to CO, benzene, toluene, and H_2. The present study shows that coating metal oxides with Si can enhance their sensing response and decrease the optimal sensing temperature.

ACKNOWLEDGMENTS

This research was supported by the Basic Science Research Program through the National Research Foundation of Korea (NRF) funded by the Ministry of Education (2016R1A6A1A03013422). This work was also supported by the NRF grant funded by the Korean government (MSIT; 2019R1A2C1006193) and this work was also supported by the research fund of Hanyang University (HY-2019).

REFERENCES

1. R. Lee, M. H. Jo, T. W. Kim, H. J. Kim, and J. C. Shin, *Electron. Mater. Lett.* **14**, 357 (2018).
2. A. Mirzaei, S. Park, H. Kheel, G.-J. Sun, S. Lee, and C. Lee, *Ceram. Int.* **42**, 6187 (2016).
3. J. H. Lee, Y. S. Park, M. J. Jang, S. M. Park, K. H. Lee, W. S. Choi, S. M. Choi, and Y. D. Kim, *Korean, J. Met. Mater.* **56**, 885 (2018).
4. S. V. N. T. Kuchibhatla, A. S. Karakoti, D. Bera, and S. Seal, *Prog. Mater. Sci.* **52**, 699 (2007).
5. J. Chen, L. N. Xu, and W. Y. Li, *Adv. Mater.* **17**, 582 (2005).
6. M. Xu and J. Zhao, *Electron. Mater. Lett.* **14**, 499 (2018).
7. Z. Wen, S. Ci, S. Mao, S. Cui, G. Lu, K. Yu, S. Luo, Z. He, and J. Chen, *J. Power Sources* **234**, 100 (2013).
8. S.-J. Choi and I.-D. Kim, *Electron. Mater. Lett.* **14**, 221 (2018).
9. X. Chen, C. K. Y. Wong, C. A. Yuan, and G. Zhang, *Sens. Actuators B-Chem.* **177**, 178 (2013).
10. J. Liao, Z. Li, G. Wang, C. Chen, S. Lv, and M. Li, *Phy. Chem. Chem. Phys.* **18**, 4835 (2016).
11. C. R. Field, H. J. In, N. J. Begue, and P. E. Pehrsson, *Anal. Chem.* **83**, 4724 (2011).
12. S. Kim, J. H. Bang, M. S. Choi, W. Oum, A. Mirzaei, N. Lee, H.-C. Kwon, D. Lee, H. Jeon, S. S. Kim, and H. W. Kim, *Met. Mater. Int.* **25**, 805 (2019).
13. H. S. Woo, C. H. Kwak, I. D. Kim, and J. H. Lee, *J. Mater. Chem. A* **2**, 6412 (2014).
14. L. L. Wang, L. P. Kang, H. Y. Wang, Z. P. Chen, and X. J. Li, *Sens. Actuators B-Chem.* **229**, 513 (2016).
15. G.-J.Sun, J. K. Lee, W. I. Lee, R. P. Dwivedi, C. Lee, and T. Ko, Electron. *Mater. Lett.* **13**, 260 (2017).
16. H. W. Kim, H. G. Na, Y. J. Kwon, H. Y. Cho, and C. Lee, *Sens. Actuators B-Chem.* **219**, 22 (2015).
17. V. Srivastava and K. Jain, *Mater. Lett.* **169**, 28 (2016).
18. A. Mirzaei, S. G. Leonardi, and G. Neri, *Ceram. Int.* **42**,

15119 (2016).
19. G. Neri, A. Bonavita, G. Micali, N. Donato, F. A. Deorsola, P. Mossino, I. Amato, and B. De Benedetti, *Sens. Actuators B-Chem.* **117**, 196 (2006).
20. S. S. Kim, H. G. Na, H. W. Kim, V. Kulish, and P. Wu, *Sci. Rep.* **5**, 1 (2015).
21. S.-W. Choi, A. Katoch, G.-J. Sun, J.-H. Kim, S.-H. Kim, and S. S. Kim, *ACS Appl. Mater. Interfaces* **6**, 8281 (2014).
22. S. Ozdemir and J. L. Gole, *Curr. Opin. Solid State Mater. Sci.* **11**, 92 (2007).
23. Y. F. Zhang, Y. H. Tang, N. Wang, D. P. Yu, C. S. Lee, I. Bello, and S. T. Lee, *Appl. Phys. Lett.* **72**, 1835 (1998).
24. W. Zhang, M. Hu, X. Liu, Y. Wei, N. Li, and Y. Qin, *J. Alloy. Compd.* **679**, 391 (2016).
25. X. Liu, M. Hu, Y. Wang, J. Liu, and Y. Qin, *J. Alloy. Compd.* **685**, 364 (2016).
26. H. W. Kim and S. H. Shim, *J. Korean Phys. Soc.* **47**, 516 (2005).
27. H. W. Kim, J. W. Lee, S. H. Shim, and C. Lee, *J. Korean Phys. Soc.* **51**, 198 (2007).
28. D. T. T. Le, D. D. Trung, N. D. Chinh, B. T. Thanh, H. S. Hong, N. Van Duy, N. D. Hoa, and N. Van Hieu, *Curr. Appl. Phys.* **13**, 1637 (2013).
29. S. Park, S. Kim, G.-J. Sun, S. Choi, S. Lee, and C. Lee, *Ceram. Int.* **41**, 9823 (2015).
30. S. An, *J. Thermodyn. Catal.* **8**, 1000186 (2017).
31. S. Park, S. Park, J. Jung, T. Hong, S. Lee, H. W. Kim, and C. Lee, *Ceram. Int.* **40**, 11051 (2014).
32. P. S. Shewale, Y. S. Yu, J.-H. Kim, C. R. Bobaded, and M. D. Uplane, *J. Anal. Appl. Pyrolysis* **112**, 348 (2015).
33. D. L. Feucht, *J. Vac. Sci. Technol.* **14**, 57 (1977).
34. M. N. Islam and M. O. Hakim, *J. Mater. Sci. Lett.* **5**, 63 (1986).
35. R. G. Gordon, *MRS Bull.* **25**, 52 (2000).
36. S. Gubbala, H. B. Russell, H. Shah, B. Deb, J. Jasinski, H. Rypkema, and M. K. Sunkara, *Energy Environ. Sci.* **2**, 1302 (2009).
37. J.-H. Kim, H. W. Kim, and S. S. Kim, *Sens. Actuators B-Chem.* **239**, 578 (2017).
38. S.-W. Choi, A. Katoch, J. Zhang, and S. S. Kim, *Sens. Actuators B-Chem.* **176**, 585 (2013).
39. S.-W. Choi, A. Katoch, G.-J. Sun, and S. S. Kim, *Sens. Actuators B-Chem.* **181**, 787 (2013).
40. J. Y. Park, S.-W. Choi, and S. S. Kim, *J. Phys. D. Appl. Phys.* **44**, 205403 (2011).
41. A. Katoch, Z. U. Abideen, H. W. Kim, and S. S. Kim, *ACS Appl. Mater. Interfaces* **8**, 2486 (2016).
42. J.-H. Kim, P. Wu, H. W. Kim, and S. S. Kim, *ACS Appl. Mater. Interfaces* **8**, 7173 (2016).
43. S.-W. Choi, A. Katoch, J.-H. Kim, and S. S. Kim, *ACS Appl. Mater. Interfaces* **6**, 17723 (2014).
44. Y. J. Kwon, H. G. Na, S. Y. Kang, M. S. Choi, J. H. Bang, T. W. Kim, A. Mirzaei, and H. W. Kim, *Sens. Actuators B-Chem.* **239**, 180 (2017).
45. J.-H. Kim, J.-H. Lee, A. Mirzaei, H. W. Kim, and S. S. Kim, *Sens. Actuators B-Chem.* **248**, 500 (2017).
46. M. Batzill and U. Diebold, *Prog. Surf. Sci.* **79**, 47 (2005).
47. X. Fang, J. Yan, L. Hu, H. Liu, and P. S. Lee, *Adv. Funct. Mater.* **22**, 1613 (2012).
48. R. S. Becker, G. S. Higashi, Y. J. Chabal, and A. J. Becker, *Phys. Rev. Lett.* **65**, 1917 (1990).
49. L. Hao, Y. Liu, W. Gao, Y. Liu, Z. Han, L. Yu, Q. Xue, and J. Zhu, *J. Alloy. Compd.* **682**, 29 (2016).
50. X. Li, H. Zhu, K. Wang, A. Cao, J. Wei, C. Li, Y. Jia, Z. Li, X. Li, and D. Wu, *Adv. Mater.* **22**, 2743 (2010).
51. R. M. Feenstra, J. A. Stroscio, and A. P. Fein, *Surf. Sci.* **181**, 295 (1987).
52. P. Dwivedi, N. Chauhan, P. Vivekanandan, S. Das, D. S. Kumar, and S. Dhanekar, *Sens. Actuators B-Chem.* **249**, 602 (2017).
53. D. Yan, S. Li, S. Liu, M. Tan, and M. Cao, *J. Alloy. Compd.* **735**, 718 (2017).
54. W. Yan, M. Hu, D. Wang, and C. Li, *Appl. Surf. Sci.* **346**, 216 (2015).
55. W. Yan, M. Hu, J. Liang, D. Wang, Y. Wei, W. Zhang, and Y. Qin, *Mater. Res. Bull.* **83**, 453 (2016).
56. Y. Qin, Z. Cui, T. Zhang, and D. Liu, *Sens. Actuators B-Chem.* **258**, 246 (2018).
57. A. Kobayashi, F. Grey, R. S. Williams, and M. Aono, *Science* **259**, 1724 (1993).
58. L.-W. Wang and A. Zunger, *J. Chem. Phys.* **100**, 2394 (1994).
59. H. Tai, X. Xu, Z. Ye, C. Liu, G. Xie, and Y. Jiang, *Chem. Phys. Lett.* **621**, 58 (2015).
60. Y. Liu, L. Hao, W. Gao, Z. Wu, Y. Lin, G. Li, W. Guo, L. Yu, H. Zeng, J. Zhu, and W. Zhang, *Sens. Actuators B-Chem.* **211**, 537 (2015).
61. I. Barin, *Thermochemical Data of Pure Substances, 3rd ed.*, Wiley, New Jersey (1997).
62. R. Lee, M. H. Jo, T. W. Kim, H. J. Kim, and J. C. Shin, *Electron. Mater. Lett.* **14**, 357 (2018).